

A Central pattern generator to control a pyloric-based system

R. Huerta^{1,2}, M.A. Sánchez-Montañés¹, F. Corbacho¹, J.A. Sigüenza¹

¹ Grupo de Neucomputación Biológica (GNB), E.T.S. de Ingeniería Informática, Universidad Autónoma de Madrid, E-28049 Madrid, Spain

² Institute for Nonlinear Science, UCSD, La Jolla, CA 92093-0402, USA

Received: 23 September 1998 / Accepted in revised form: 11 June 1999

Abstract. A central pattern generator (CPG) is built to control a mechanical device (plant) inspired by the pyloric chamber of the lobster. Conductance-based models are used to construct the neurons of the CPG. The plant has an associated function that measures the amount of food flowing through it per unit of time. We search for the best set of solutions that give a high positive flow of food in the maximization function. The plant is symmetric and the model neurons are identical to avoid any bias in the space of solutions. We find that the solution is not unique and that three neurons are sufficient to produce positive flow. We propose an effective principle for CPGs (effective on-off connectivity) and a few predictions to be corroborated in the pyloric system of the lobster.

1 Introduction

A central pattern generator (CPG) is a network of neurons that generates a coordinated rhythmic activity to control a part of the body of the animal to perform a specific motor function such as chewing, swimming, walking, and so on (Delcomyn 1980; Marder and Calabrese 1996). CPGs correspond to small groups of synaptically coupled neurons with autonomous activity, that is, produced without the need for sensory feedback. In general the CPG motor neurons control a set of muscles in the animal. We will call this part of the body of the animal that performs a set of predefined functions a *plant*. We borrow the term plant from control theory, where a plant is defined as the physical system to be controlled. The CPG conveys control information to the plant to carry out its functionality in the best possible manner. In this paper the plant will be a mechanical model based on the lobster pylorus, although we present general principles that may apply to other plants.

Many researchers have worked out the structure of some CPGs in animals such as *Clione* (Arshavsky et al. 1985), *Tritonia* (Katz et al. 1994), lobster (Selverston and Moulins 1987), leech (Brodfuehrer et al. 1995), lamprey (Grillner et al. 1995), locust (Wolf and Laurent 1994), and others. Many questions have been answered about the connectivity, phase patterns, and effects of neuromodulators in the spatiotemporal patterns, yet it still remains extremely difficult to measure simultaneously the muscle activity and the electrical activity of the CPG. This fact has led to the development of CPG models isolated from models of the plants they control in the living animal. Although there is general agreement that the interaction with the mechanical environment plays a crucial role in the normal operation of the neuronal control system (Ekeberg et al. 1995), there is a much more reduced body of literature concentrating on the relation between the electrical activity of the CPG and the dynamics of the plant (Sigvardt and Mulloney 1982; Katz and Harris-Warrick 1990; Ryckebusch and Laurent 1994; Bohm 1996; Shaw and Kristan 1997; Clemens et al. 1998). Even at the theoretical level, there are few research efforts that try to solve this relation (Cohen et al. 1992; Hatsopoulos 1996; Wadden et al. 1997; Zielinska 1996). Most of these investigations are not fully based on CPGs, because they lack a complete description of the CPG connectivity and the units are modeled by oscillators far from a conductance-based model.

Grillner and colleagues (Ekeberg 1993; Ekeberg et al. 1995) among others (Müller-Wilm et al. 1992; Cruse et al. 1995a,b; Hatsopoulos 1996) represent one of the few exceptions with their work on what they have defined as a neuromechanical model. They claim that many simulations done thus far incorporate only the neuronal pattern generator, hence leaving a gap between the simulation results and the experimental studies of the corresponding behavior in the real animal. They bridge this gap by extending the simulation model to include also the muscular generation of the movements, thereby verifying that the motor patterns produced actually correspond to the expected real movements.

In this paper we intend to study a specific example based on the crustacean stomatogastric system, which is, one of the best-described systems (Selverston and Moulins 1987). We are not just going to concentrate on the family of phase patterns generated by a particular model of the CPG and its analysis with respect to the experimental recordings (Ryckebusch and Laurent 1993; Collins and Stewart 1994; Ryckebusch 1994; Ryckebusch and Laurent 1994; Huerta 1996; Roberts 1997). We will also study the relationship between the phase pattern and its functionality on the plant. We are guided by the next set of questions: Why do we find a particular number of neurons in a CPG? What is the role of a particular connectivity pattern? Is there a unique solution for a given connectivity pattern?

We start by building a plant inspired by the pyloric chamber of the lobster and a CPG with conductance-based neurons. Once we have found the dynamic equations governing the plant we explore the minimum necessary network to achieve a goal. We postulate a function that establishes the criteria to maximize the activity of the network. Our assumption is that, in this particular plant (“pylorus”), the network maximizes the total amount of food leaving the pylorus per unit of time. In this way, the information conveyed by the spatiotemporal pattern generated by the CPGs is measured with respect to this maximization function. Moreover, although we are aware that the pylorus in the lobster is nonsymmetric we design a complete symmetric plant. We would like to show that a set of optimal solutions exist regardless of the natural asymmetry in biological systems. This means that given a family of solutions that optimize the process for a symmetric problem, we can modify the parameters of the plant (areas, lengths, and elasticity constants) to enhance the best solutions. Therefore, the model of the plant has no preferred direction. We proceed in the same manner to model the neurons in the network utilizing exactly the same dynamics for all the neurons. It is well known that neurons in the pyloric CPG are rather different. (Selverston and Moulins 1987). The duration of the bursts of the lateral pyloric (LP), posterior dilator (PD) and pyloric neuron (PY) are different. A reasonable hypothesis is that evolution or rather development modifies the dynamic characteristics of the neurons to facilitate the function of the plant. Our starting point is not to set any a priori asymmetry that will quickly provide the best solution. The search of the best parameters in the maximization function points at the asymmetries that will enhance the response of the plant.

An increasingly voiced concern among neuroscientists is that although enormous advances in knowledge of cellular and synaptic phenomena have occurred in the last decade, insights into the organizational principles of neural and behavioral function remain few (Schöner 1995). Therefore, as Grillner (1997) points out, a major challenge for neuroscience is to bridge the gap between molecular-cellular events and behavior. He continues arguing that even a complete molecular description of each cell of the central nervous system (CNS) would not describe its functions, because the essence of the CNS is

its intricate organization. In this paper we follow that direction by searching for connectivity patterns and underlying principles that give rise to the maximization of functionals. Concretely, as already mentioned, we have searched for configurations that maximize the flow.

To be able to understand how the nervous system generates behavior, with the nerve cells as the building blocks, one needs to work on all neural levels of organization from molecule, cell, and synapse to network and behavior (Schöner and Kelso 1988; Grillner 1997). Yet it is difficult to extrapolate from the large number of specific examples of experimental data to general principles of organization. Hence, the challenge is to create links between these different levels and to find simple model preparations appropriate for the particular behavior of interest. Although we do not claim to have found a complete set of principles bridging across all levels, we provide a set of principles of organization coherent with the work presented here and learned in the process of analyzing the interactions of the CPG with the plant. In the discussion section we also elaborate on the commonalities of structure and physiology that begin to shed a light on general principles of motor organization that may apply across different species.

2 The system

The system is composed of two main parts: the plant, and the CPG. The first is the mechanical device that interacts with the fluid, that is, the pyloric chamber. We model it by three joint pipes that are elastic in the radial direction (see Fig. 1). Each of these pipes is controlled by one neuron and all these neurons can be connected to each other. Pressures at both sides of the plant, P_1 , P_6 , are identical to keep a symmetric problem. Our assumption is that this plant is driven by the CPG, which attempts to maximize the average flow of food leaving it per unit of time. The real pylorus of the lobster appears

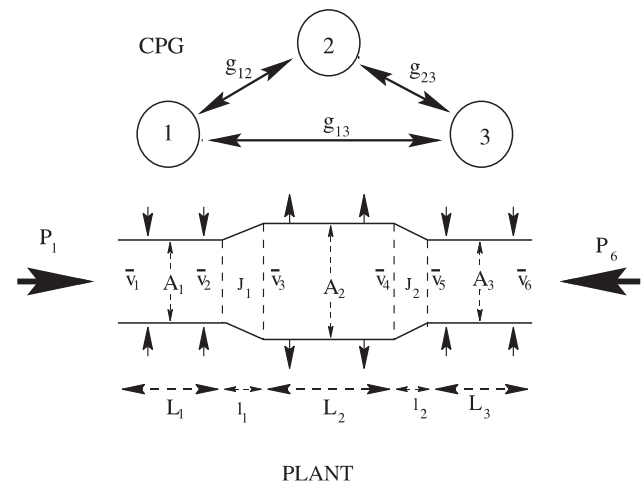


Fig. 1. The type of problem to be solved in this paper. On the *upper part* we use three identical neurons that can be interconnected in any possible way. On the *lower part*, the plant is shown. Each neuron only affects one section of the plant

to be filtering food; a better description would be given then not by the maximum flow but by the ‘‘proper’’ velocity of the flow; however for the simplicity of our equations we disregard this additional term. The maximization function we used is described by

$$\Phi = \frac{\rho}{T} \int_0^T A_3(t) \bar{v}_6(t) dt, \quad (1)$$

where T is the averaging time, ρ is the density of the viscous fluid, A_3 is the area of the section of the third pipe, and \bar{v}_6 is the average speed at the end of the plant. The plant and the CPG were integrated using a Runge-Kutta 6(5) scheme with variable time step with an absolute error of 10^{-16} and a relative error of 10^{-6} .

2.1 Plant equations

The plant equations are derived from the Navier-Stokes mass and energy conservation equations under the assumptions that the food is homogeneous, incompressible, and isothermal with a dynamics in the laminar regimen (low Reynolds number) and small radial velocities. We also assume no food leaks through the membrane, because we only considered a maximization function that measures the flow through the pipes.

In Appendix 1, we explain how we obtain a set of ordinary differential equations (ODEs) that gives the temporal evolution of the mean velocity through a cross section at both ends and at the joints of the plant. The simplification of the plant equations to a set of ODEs can be linked with the neuron ODEs to be integrated in an efficient manner. To express the ODE in a compact manner we will set $y_0 = A_1, y_2 = A_2, y_5 = A_3, y_1 = \bar{v}_1, y_3 = \bar{v}_3, y_4 = \bar{v}_4, y_6 = \bar{v}_6$, which gives

$$\dot{y}_0 = \frac{y_0(y_1 - \bar{v}_2)}{L_1},$$

$$\dot{y}_1 = \frac{-107\bar{v}_2^2 + 53y_1^2 + 54\bar{v}_2y_1}{96L_1} - \frac{3(2P_{\text{ext}1} - P_1 - P_2)L_1\pi}{2y_0\rho} + \frac{P_1 - P_2}{\rho L_1} - \mu \frac{(\bar{v}_2 + 7y_1)\pi}{y_0\rho},$$

$$\dot{y}_2 = \frac{y_2(y_3 - y_4)}{L_2},$$

$$\dot{y}_3 = \frac{-107y_4^2 + 53y_3^2 + 54y_4y_3}{96L_2} - \frac{3(2P_{\text{ext}2} - P_3 - P_4)L_2\pi}{2y_2\rho} + \frac{P_3 - P_4}{\rho L_2} - \mu \frac{(y_4 + 7y_3)\pi}{y_2\rho},$$

$$\dot{y}_4 = \frac{-53y_4^2 + 107y_3^2 - 54y_4y_3}{96L_2} + \frac{3(2P_{\text{ext}2} - P_3 - P_4)L_2\pi}{2y_2\rho} + \frac{P_3 - P_4}{\rho L_2} - \mu \frac{(7y_4 + y_3)\pi}{y_2\rho},$$

$$\dot{y}_5 = \frac{y_5(\bar{v}_5 - y_6)}{L_3},$$

$$\dot{y}_6 = \frac{-53y_6^2 + 107\bar{v}_5^2 - 54y_6\bar{v}_5}{96L_3} + \frac{3(2P_{\text{ext}3} - P_5 - P_6)L_3\pi}{2y_5\rho} + \frac{P_5 - P_6}{\rho L_3} - \mu \frac{(7y_6 + \bar{v}_5)\pi}{y_5\rho},$$

where $L_1 = L_2 = L_3 = 1$ cm, $P_1 = P_6 = 10^6$ dyne/cm², $\rho = 1$ g/cm³ (water density), $\mu = 0.013$ g/cm per second (water dynamic viscosity at 10 °C). The term lead by μ is dissipative and is due to the viscosity of the fluid.

The pressures P_2, P_3, P_4 and P_5 are determined from the mass and energy conservation at both joints under the assumption of smooth joints (no head-loss). The conservation equations are

$$v_2 = \frac{y_3y_2}{y_0} \quad (\text{mass conservation at } J_1) \text{ as seen in Fig. 1}$$

$$v_5 = \frac{y_4y_2}{y_5} \quad (\text{mass conservation at } J_2)$$

$$P_2 = P_3 + \frac{1}{2}\rho \left(y_3^2 - \frac{y_3^2y_2^2}{y_0^2} \right) \quad (\text{energy conservation at } J_1)$$

$$P_5 = P_4 + \frac{1}{2}\rho \left(y_4^2 - \frac{y_4^2y_2^2}{y_5^2} \right) \quad (\text{energy conservation at } J_2)$$

The explicit equations for P_2, P_3, P_4 , and P_5 are long expressions. They have been calculated using a programming language for symbolic manipulation.

The external pressure is the sum of the atmospheric pressure, the elastic pressure exerted by the walls of the plant, the muscle pressure, and the damping force due to the dissipation of the muscles. It can be expressed as

$$P_{\text{ext}i} = \frac{(P_1 + P_6)}{2} + P_i^{\text{elastic}} + P_i^{\text{muscle}} + bv_{ri},$$

where P_i^{elastic} is the elastic pressure and it was calculated assuming a ring of springs linked by the ends that offers a radial force into the fluid. The expression is

$$P_i^{\text{elastic}} = K \left(1 - \frac{\sqrt{A_i^0}}{\sqrt{A_i(t)}} \right) \theta(A_i(t) - A_i^0)$$

where $K = 80$ dyne/cm², the resting values of the sections of the pipes are $A_1^0 = A_2^0 = A_3^0 = 0.5$ cm². The elastic pressure has a Heaviside function multiplying it because when the muscle compresses the pipe below the resting area the membrane does not oppose any force. The radial velocity of the pipe is given by

$$v_{ri} = -\frac{\sqrt{A_i(t)}(\bar{v}_{2i} - \bar{v}_{2i-1})}{2\sqrt{\pi}L},$$

where the damping constant is $b = 120$ g/cm² per second. This parameter value has been set to a

sufficiently large value to avoid oscillations of the pipe for a period longer than one second.

The pressure exerted on the pipe, P_i^{muscle} is given by Hooke's law, equivalent to the elastic force of the pipe given above. We write it as

$$P_i^{\text{muscle}} = \eta \left(1 - \frac{f(\alpha(V_m + 65(\text{mV})))}{\sqrt{A_i(t)}} \right),$$

where V_m is the electrical activity of the muscle (see Appendix 2), $\eta = 400 \text{ dyne/cm}^2$, $\alpha = 1 \text{ dyne/cm}^2 \text{ mV}$ and

$$f(p) = \sqrt{A_i^0} \left((1 - \kappa) + \frac{\kappa}{1 + e^{(p-p_c)/\sigma}} \right),$$

with $\sigma = 0.4 \text{ dyne/cm}^2$, $p_c = 10 \text{ dyne/cm}^2$, $\kappa = 0.2$ for contracting muscles and $\kappa = -0.2$ for dilator muscles. The function $f(x)$ is a sigmoidal function that gives the resting length corresponding to the electrical activity of the springlike muscle (see Kandell et al. 1991). There are wide ranges of parameter values for the muscle activity that produce the same qualitative results. The most important parameter is the dimensionless κ that determines the amount of opening and closing section of the pipe. This parameter value cannot be increased at will due to the assumption of small radial velocities.

2.2 The model of the neurons

This model is based on Turrigiano et al. (1995) and Falcke et al. (1999) but without the complex calcium dynamics, which is necessary to provide consistent chaotic behavior as observed in physiological recordings. The calcium dynamics in the endoplasmic reticulum in the Falcke model has a very low time scale, which entails that very long transients are required to reach an attractor. These long transients need long integration times that are too costly for our computational capabilities. Hence, we used a first-order kinetic equation for the calcium dynamics as in Turrigiano et al. (1995). The model consists of two compartments, one for the axon (fast generator) and another for the neuropil and soma (the slow generator). The fast generator provides the spikes with the help of a sodium current I_{Na} , a delayed rectifier potassium current I_{Kd} , and a leakage current I_{Lf} . We write it as

$$C_m^{\text{axon}} \dot{V}_f = -I_{\text{Na}} - I_{\text{Kd}} - I_{\text{Lf}} + I_{V_f, V_s},$$

where $C_m^{\text{axon}} = 0.33 \text{ nF}$, V_f is the membrane potential in the axon, and V_s is the membrane potential of the neuropil and soma. The slow dynamics is provided by

$$C_m^{\text{soma}} \dot{V}_s = -I_{\text{Ca}} - I_{\text{Ls}} - I_{\text{h}} - I_{\text{K(Ca)}} - I_{V_f, V_s} + I^{\text{syn}} + I_{\text{dc}},$$

where $C_m^{\text{soma}} = 0.5 \text{ nF}$, I_{Ca} is the calcium current, I_{Ls} the leakage current, I_{h} is a low threshold current, $I_{\text{K(Ca)}}$ is the potassium calcium dependent current, I_{dc} is the injected current, I_{V_f, V_s} is the current connecting both

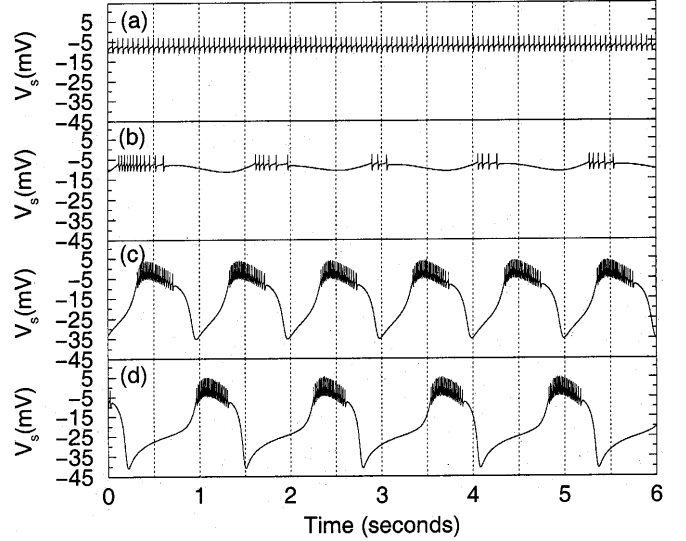


Fig. 2. Membrane potentials in the soma for the model neuron for different values of the injected current: (a) $I_{\text{dc}} = 4 \text{ nA}$, (b) $I_{\text{dc}} = 3.4 \text{ nA}$, (c) $I_{\text{dc}} = 0 \text{ nA}$, and (d) $I_{\text{dc}} = -2 \text{ nA}$

compartments, and I_{syn} is the synaptic current, which will be explained below. All these currents are described in Appendix 2.

The calcium dynamics is described by the following first-order kinetic equation:

$$[\dot{\text{Ca}}] = -\alpha I_{\text{Ca}} - \beta [\text{Ca}] + \gamma,$$

with $\alpha = 6.6 \cdot 10^{-5} \text{ } \mu\text{M/ms per nA}$, $\beta = 1.21 \cdot 10^{-3} \text{ ms}^{-1}$, $\gamma = 4.84 \cdot 10^{-5} \text{ } \mu\text{M/ms}$, and $[\text{Ca}]$ has units of μM .

In Fig. 2 we show time traces of this neuron for different values of the injected current. We can see that as the injected current is increased the neuron decreases the period until it reaches the spiking behavior. This behavior reproduces the qualitative standard behavior of the LP neurons in the pyloric ganglia (Abarbanel et al. 1996; Golowasch and Marder 1992).

The synaptic current, I^{syn} , is given by

$$I_i^{\text{syn}} = g_{ij} r_j(t) (V_s(i) + 70 \text{ mV}),$$

where i stands for the index of the neuron from which the synaptic input is received, j is the neuron that receives the synaptic input, and r_j is the fraction of bound receptors (Destexhe et al. 1994). The connectivity between neurons is the most important parameter; the maximal conductances g_{ij} will mainly determine the whole behavior of the network.

To model the muscle activity we used a very simple dynamics that would be classified within the input-output models according to Krylow et al. (1995). We used a passive circuit that receives excitatory post synaptic potential (EPSP) from the motor neurons. If we compare the electromyography (EMG) recordings from the pyloric muscles in vivo (Selverston and Moulins 1987; Clemens et al. 1998), the electrical activity in the muscles is highly correlated to the neuron activities. We model the muscle activity according to this observation.

A wide variety of motor tasks reveal correlations between features of the EMG record and task parameters (Sherwood et al. 1988; Gottlieb et al. 1992). However, the neural mechanisms for the control of the muscle activity is poorly understood due to the complexity of the premotor and motor circuits involved (Morris and Hooper 1998). Besides, in most cases, the mapping from motor neuron activity to muscle dynamics is not known to any good degree of precision. On the other hand the pyloric CPG contains a much more reduced number of motor neurons within simpler configurations. Hence this results in EMG characteristics, for example, onset time, rising rate, peak amplitude, duration, total activation, and decay rate that are correlated to motor neuron activity to a greater degree than in other CPG preparations.

4 Effective On-off connectivity

The parameter space that we explore in order to maximize the total flow given by Eq. 1 is limited to the inhibitory synaptic connections. We did not include excitatory synapses because they typically generate in-phase oscillations, and CPGs very rarely present them (Selverston and Moulins 1987). We do not completely rule out their influence in the maximization function; however inhibitory synapses are mainly responsible for organizing phase shifts in the oscillations of the CPGs. Therefore, it does not seem that excitatory synapses will importantly affect the outcome of the plant and their absence in our simulations allows us to reduce the searching space.

To further check the variability with the strength of the synaptic connections we used the reduced solution given by the circuit shown in Fig. 3. We set the value of the connections as $g_{12} = g_{13} = g_{21} = g_{23} = g_{31} = 0.05 \mu\text{S}$ and $g_{32} = 0 \mu\text{S}$. Then we choose one of the connectivities and modify its value from 0 to $0.2 \mu\text{S}$. The system was integrated for 60 s with initial conditions $\bar{v}_1 = \bar{v}_2 = \bar{v}_3 = \bar{v}_4 = \bar{v}_5 = \bar{v}_6 = 0$ in the pylorus. For each value of g_{ij} 15

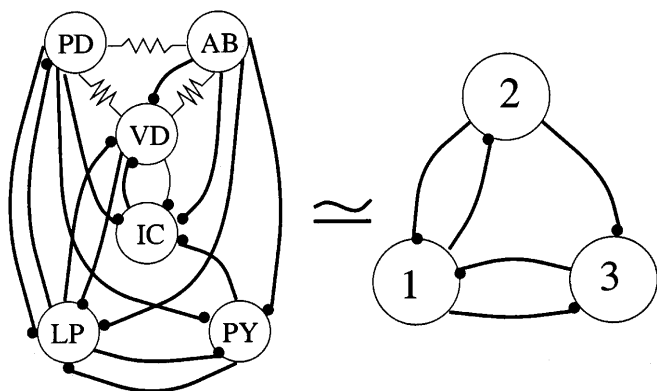


Fig. 3. On the left, pyloric CPG (Selverston and Moulins 1985). On the right, reduced equivalent circuit as required by our circuit proposed in Fig. 1. Neuron 1 is equivalent to LP, neuron 3 is equivalent to the neurons PY, neuron 2 is the group AB-PD responsible for dilating the central pipe

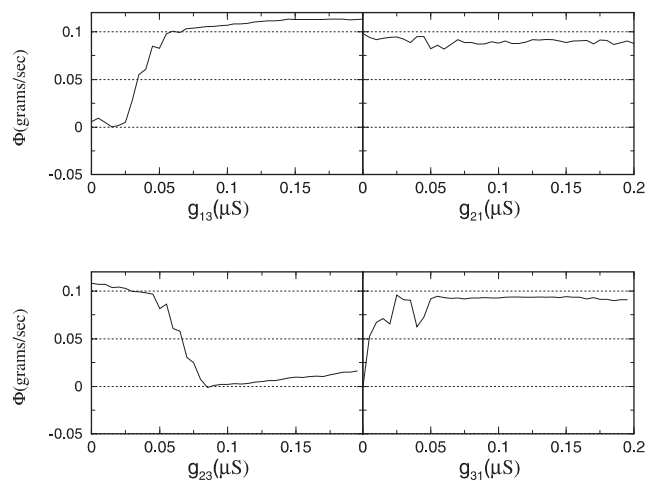


Fig. 4. Total flow as a function of the strength of one of the synaptic parameters for the solution $g_{12} = g_{13} = g_{21} = g_{23} = g_{31} = 0.05 \mu\text{S}$, and $g_{32} = 0 \mu\text{S}$, which is based on the pyloric circuit (see Fig. 3)

different initial conditions were utilized and the average value was used for comparison. In Fig. 4 we can see the value of Φ that either remains close to 0.1 g/s or near 0. The maximization of the flow of food stays more or less constant until it reaches a threshold value. Therefore we can speak of an on-off connectivity, because what is important for the system is not the actual value but whether g is above or below the critical one. Some predictions that can be derived from Fig. 4 are

1. The connection g_{21} is not necessary to maximize the flow in the plant.
2. In connection g_{23} is strongly increased then the plant does not work.

5 Search for solutions

A systematic search in the connectivity space to find the best set of solutions requires large computation time (six connections and 20–40 trials for different initial conditions). However, the observation made in the previous section tells us that there is a small variation of the maximization function until threshold values are reached. It is reasonable to expect that small variations of the parameters do not substantially change the behavior of the CPG because robustness is one of the main characteristics of biological systems. We use the presence of this on-off connectivity to explore a space of 2^6 possible configurations (where each g_{ij} can be either on or off). This is an advantage for our computational limitations, although we are aware that we might be missing some relevant information in the fine detail of the strengths of the coupling.

We mainly studied the case in which the central muscle is dilating because in the pyloric chamber the PD neurons are responsible for dilating the central part; we will denote this solution by $(+ - +)$. Moreover we also studied the case when the central muscle is compressing

the central pipe (solution + + +) to distinguish whether there is any advantage of this specific type of solution.

After performing a set of simulations we can classify the solutions by the following definitions:

1. Open topology: if there is at least one neuron in the network that does not receive any synaptic input from any other neuron
2. Semi-open topology: if there is at least one neuron in the network that does not send a synaptic input to any other neuron in the network
3. Closed topology: if all neurons in the network receive *and* send at least one connection to any other neuron in the network

We have found solutions that maximize the flow for all three categories; however, since we have been using a neuron that behaves rather regularly we have been unable to check the robustness of these different solutions. To test these solutions further chaotic neurons are required. We test system robustness by introducing white noise at the level of the injected current I_{dc} , but the limit cycles are strongly dissipative and any perturbation is rapidly driven to the limit cycle. Therefore, the open topology solutions remain good. It is known that for chaotic bursting oscillators mutual inhibition is required to regularize their behavior (Abarbanel et al. 1996; Rabinovich et al. 1997). It has been seen experimentally that the LP and the PD neurons in the pyloric system regularize their behavior by mutual inhibition (Elson et al. in press). Therefore, the open and semiopen topologies are unlikely to exist.

For the (+ - +) solutions there are 13 configurations that produce a flow over 0.07 g/s. One of them is semiopen, 7 of them are open and 5 are closed. The closed-topology solutions are given in Table 1. The last solution (*) in Table 1 corresponds to the solution based on the connections found in the real pyloric system. It is among the optimal solutions, although it is not the best. Figure 5 displays the membrane potential for the three neurons in the CPG as well as the total flow as a function of time corresponding to the best solution: $g_{12} = g_{13} = g_{23} = g_{31} = 0.05 \mu\text{S}$, $g_{21} = g_{32} = 0 \mu\text{S}$.

If we increase the food density from 1 to 2 g/cm³ and calculate again, we obtain 14 solutions over 0.14 g/s (twice the value used for density 1 g/cm³ by Eq. 1). Two of them are semi open and six are open, which we disregard. Five closed-topology solutions remain, which are written in Table 2.

We can see that there is a small permutation in the set of best solutions. This result tells us that depending on the type of food, a small change in the optimal topology is produced. Therefore, there is a reason for the pyloric system to have an endogenous mechanism to change the connectivity pattern to maximize the flow as a function of the type of food. We can see that the biologically based solution is still not the best. The connection g_{21} is unnecessary if we compare it to the best solution in the table (this is confirmed in Fig. 4 and is matter of discussion).

We are assuming in this paper that the pylorus is just maximizing the flow of food through it. If this were the

Table 1. (+ - +) closed-topology solutions for $\rho = 1 \text{ g/cm}^3$

Φ (g/s)	g_{12} (μS)	g_{13} (μS)	g_{21} (μS)	g_{23} (μS)	g_{31} (μS)	g_{32} (μS)
0.094	0.05	0.05	0	0.05	0.05	0
0.096	0.05	0.05	0.05	0	0	0.05
0.102	0.05	0.05	0.05	0	0.05	0
0.095	0.05	0.05	0.05	0	0.05	0.05
0.079(*)	0.05	0.05	0.05	0.05	0.05	0

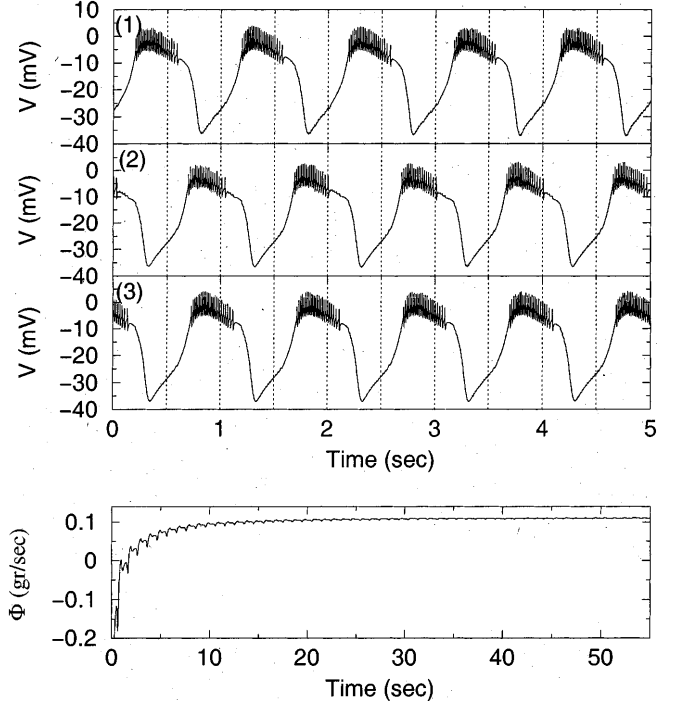


Fig. 5. Time series for the solution $g_{12} = 0.05 \mu\text{S}$, $g_{13} = 0.05 \mu\text{S}$, $g_{21} = 0 \mu\text{S}$, $g_{23} = 0.05 \mu\text{S}$, $g_{31} = 0.05 \mu\text{S}$ and $g_{32} = 0 \mu\text{S}$ for $\rho = 1 \text{ g/cm}^3$. (2) Membrane potential of the neuron 2 in our system that corresponds to the neuron PD, (1) Membrane potential of the neuron 1 that corresponds to the neuron LP and (3) corresponds to the PY neurons. On the lower panel, total flow as a function of time for this particular solution

Table 2. (+ - +) closed-topology solutions for $\rho = 2 \text{ g/cm}^3$

Φ (g/s)	g_{12} (μS)	g_{13} (μS)	g_{21} (μS)	g_{23} (μS)	g_{31} (μS)	g_{32} (μS)
0.20	0.05	0.05	0	0.05	0.05	0
0.23	0.05	0.05	0.05	0	0	0.05
0.22	0.05	0.05	0.05	0	0.05	0
0.16	0.05	0.05	0.05	0	0.05	0.05
0.19(*)	0.05	0.05	0.05	0.05	0.05	0

case one would expect that the (+ - +) solutions would be remarkably more efficient than the (+ + +) solutions, because that is what we find in the pyloric system. To test it we calculate again for $\rho = 1 \text{ g/cm}^3$ and the next set of solutions are obtained (Table 3).

The value of Φ is smaller for all these new solutions than for those obtained in Table 1. This result supports the biological solution and our maximization function. However, the improvement is not sufficiently high as to

Table 3. (+ + +) closed-topology solutions for $\rho = 1 \text{ g/cm}^3$

Φ (g/s)	g_{12} (μS)	g_{13} (μS)	g_{21} (μS)	g_{23} (μS)	g_{31} (μS)	g_{32} (μS)
0.077	0	0.05	0	0.05	0.05	0.05
0.069	0	0.05	0.05	0	0.05	0.05
0.065	0	0.05	0.05	0.05	0.05	0.05
0.076	0.05	0	0	0.05	0.05	0.05
0.054	0.05	0.05	0	0.05	0.05	0.05

state that the dilator central muscle is a necessary element in the mechanical model.

6 Discussion

As was mentioned in the introductory section, we have made an attempt to extrapolate from the specific results of this work to more general principles of interest to a wider neuroscientific audience. Next we list a few of the general lessons learned.

Principle 1. Existence of on-off synapses. For certain types of circuits – connectivity patterns – the synaptic conductance value, although a continuous value, is discretized in two regions – the on and off regions – around a critical value. The exact conductance value within a region is irrelevant and only modifications in the conductance values that take the synapse from one region to another can qualitatively affect the behavior of the system. Some of the advantages of the on-off connectivity are a reduced search space for optimal solutions and the robustness against small fluctuations within any one of the regions. In this regard the interaction of neuromodulatory substances with CPG neurons suggests that CPGs are not rigid hard-wired circuits but flexible dynamic systems, able to produce stable robust behaviors yet easily modified by sensory feedback. These systems are able to change from one state to another by simply recoding the synaptic and cellular properties of the component neurons (Harris-Warrick et al. 1995). We claim that modulation of synaptic conductances would only be effective if the modulation is able to take the conductance value from one region to another; Modulation is of vital importance to be able to optimize certain functions under different varying conditions (e.g. change in the density of the liquid going through the pylorus).

Principle 2. Existence of a family of solutions (i.e. topologies) to perform a particular function. This again gives rise to more robust systems since small lesions that may affect one solution may not affect another. Recently, it has been shown that the high reliability and flexibility of central pattern generators is determined by their redundant organization. Everything that is crucial for generator operation is determined by a number of complementary mechanisms acting in concert; however, various mechanisms are weighted differently in determining different aspects of the central pattern generator operation (Arshavsky et al. 1997).

The model predicts that by blocking synapse “21” the flow through the pylorus will not change. Nevertheless, it is expected that some other functionality will be affected. We would like at this point to introduce the next speculation. We certainly tested the dependence of the open topology solutions on the noise. We found that there was no dependence in the performance of the plant as a function of the noise. The neurons used in this CPG are highly dissipative and are not sitting close to any bifurcation. This means that any perturbation from the limit cycle will be rapidly driven back to it. The only possible way actually to test the performance of the open-topology solutions is to use chaotic neurons because the plant certainly needs regular activity to provide a positive flow. Since the only known mechanism to provide stable regular oscillations in chaotic neurons is inhibitory feedbacks (Elson et al. in press), we believe that the open-topology solutions will be disregarded.

There are few more neurons in the pyloric system, yet three neurons seem to be sufficient to produce positive flow. This raises a number of questions such as: What is the role of the other neurons? What other functions may this circuit serve? To answer these questions the coordination of the pyloric and the gastric circuit needs to be included. Then it might be found that the role of other motor neurons, not included in the model reported here, such as VD (ventricular dilator) and (inferior cardiac) IC becomes relevant.

The additional role of the pylorus as a filter deserves special attention in the future. It seems that in the pyloric region food particles may be filtered and sent to more caudal regions of the gut (Selverston and Moulins 1985). In this regard the (+ - +) solution might become even a better solution than the (+ + +) solution, since the first one increases the overall volume of the pyloric chamber and hence the contact area between the fluid and the pyloric membrane, which should in turn favor the filtering function. Plant and CPG have coevolved, or at least components of both must have evolved simultaneously.

One of the main tasks in motor control is to find what set of mechanisms gives rise to the observed behavior. Many of the questions remain at the interface between phenomena at the cell and molecular level and actual behavior. The choice of the lobster STG system to study issues in motor control is several fold. In vertebrates motor control involves the action of a much larger number of neurons and may also include more involved factors such as motivation and behavioral choice. All these aspects are orders of magnitude more complex in most vertebrates where the neural mechanisms of the control of the muscle activity are also poorly understood due to the complexity of the premotor and motor circuits involved (Liaw et al. 1994). For instance, in the mammalian respiratory CPGs the underlying rhythmic pattern of neural activity consists of three phases: inspiratory, postinspiratory, and stage-2 expiratory. The pattern results from spatial and temporal interactions of cellular and network processes that are not yet fully understood (Smith 1997). Also the

locus of the oscillator is not clear: it still remains an important problem to establish causality between the activity of oscillatory neurons found in the pre-Bötzing complex and the actual production of the rhythm.

Acknowledgements. We thank the Dirección General de Enseñanza Superior e Investigación Científica for financial support (PB97-1448). M.A.S.M. was supported by a FPU grant from MEC (Spain). We also acknowledge the CCCFC at Universidad Autónoma de Madrid for its support to this work. We want to thank Rob Elson, Al Selverston, Mikhail Rabinovich, Henry Abarbanel, and Eve Marder for stimulating discussions.

Appendix 1

The model of the pylorus consists of three joint pipes (Fig. 1). Each one of these pipes is controlled by a muscle that either pushes or pulls the pipe surface. For simplicity, we consider that the radius of each pipe is constant along its length (but not in time). Also the food traversing the pylorus is considered as an homogeneous and incompressible fluid that completely fills the plant (there is no air inside the pylorus).

We depart from the Navier-Stokes equations that describe the dynamics of a fluid in cylindric coordinates (Landau and Lifshitz 1963). Because of the symmetry of the plant, we consider that these equations only depend on t, r, z . Hence, we have two independent equations:

$$\frac{\partial v_z}{\partial t} + v_z \frac{\partial v_z}{\partial z} + v_r \frac{\partial v_z}{\partial r} = -\frac{1}{\rho} \frac{\partial P}{\partial z} + \frac{\mu}{\rho} \left(\frac{1}{r} \frac{\partial}{\partial r} \left(r \frac{\partial v_z}{\partial r} \right) + \frac{\partial^2 v_z}{\partial z^2} \right), \quad (2)$$

$$\frac{\partial v_r}{\partial t} + v_z \frac{\partial v_r}{\partial z} + v_r \frac{\partial v_r}{\partial r} = -\frac{1}{\rho} \frac{\partial P}{\partial r} + \frac{\mu}{\rho} \left(\frac{1}{r} \frac{\partial}{\partial r} \left(r \frac{\partial v_r}{\partial r} \right) - \frac{v_r}{r^2} + \frac{\partial^2 v_r}{\partial z^2} \right), \quad (3)$$

where ρ is the fluid density, μ the viscosity, v_r the radial velocity, v_z the axial one, and $P = P(z, r, t)$ is the localized pressure. The equation of mass conservation is (Landau and Lifshitz 1963)

$$\frac{1}{r} \frac{\partial}{\partial r} (rv_r) + \frac{\partial v_z}{\partial z} = 0 \quad (4)$$

We integrate it using $v_r(t, 0, z) = 0$ to obtain

$$v_r(t, r', z) = -\frac{1}{r'} \int_0^{r'} r \frac{\partial v_z(t, r, z)}{\partial z} dr \quad (5)$$

Because we are interested in describing the pipe with macroscopic variables, we will integrate Eqs. (2) and (3) in r and z to eliminate the dependence in these variables, but to do it we need first to estimate the velocity field.

Since there is no analytical solution for the Navier-Stokes equations applied to our plant, we consider the dynamics of each mobile pipe as a perturbation of the dynamics of a static pipe with laminar flow. This holds if the movement of the fluid is sufficiently smooth and the radial velocity is not too high; these are both reasonable assumptions for this plant. The velocity flow of a viscous fluid in the laminar regime for a static pipe (i.e. the radius of the pipe is not dependent on time) is the Poiseuille flow (Giles et al. 1994), which is described by

$$v_z(t, r, z) = 2\bar{v}(t, z) \left(1 - \frac{r^2}{R^2} \right) \quad \text{and} \quad v_r(t, r, z) = 0, \quad (6)$$

where $\bar{v}(z, t)$ is defined as the mean velocity through a cross section of the pipe at z and time t with R the radius of the pipe. Since we make the radial velocity of our plant lower than the axial velocity, we consider that the radial velocity only introduces a small perturbation into these equations and, therefore, the axial velocity equation remains quadratic. To calculate the radial velocity we use Eq. (5), which yields

$$v_z(t, r, z) = 2\bar{v}(t, z) \left(1 - \frac{r^2}{R(t)^2} \right), \quad (7)$$

$$v_r(t, r, z) = -\frac{\partial \bar{v}(t, z)}{\partial z} \left(r - \frac{r^3}{2R(t)^2} \right) \quad (8)$$

This is the velocity flow that approximately describes the dynamics of the plant. It is not an analytical solution of the Navier-Stokes equation, but since we are considering small perturbations of the cross section of the pipe it will help us notably to simplify the equations.

Macroscopic version of Eq. (4) for a pipe

Now we consider the conservation of mass through a cross section of the pipe or joint, which is obtained by multiplying Eq. (4) by $2\pi r$ and is then integrated in r . Using $u_r(t, 0, z) = 0$ and $v_r(t, R(t), z) = \dot{R}(t)$ we get

$$2 \frac{\dot{R}(t)}{R(t)} + \frac{\partial \bar{v}(t, z)}{\partial z} = 0 \quad (9)$$

To obtain $\bar{v}(t, z)$ in a pipe we integrate Eq. (9) along it and simplify to express $\dot{R}(t)$ as

$$\dot{R}(t) = -\frac{R(t)}{2L} (\bar{v}_L(t) - \bar{v}_0(t)), \quad (10)$$

where $\bar{v}_0(t) = \bar{v}(t, 0)$ and $\bar{v}_L(t) = \bar{v}(t, L)$ are the mean velocity at the beginning and the end of the pipe. Equation (10) shows that the distribution of $\bar{v}(t, z)$ is linear in z , which can be written as

$$\bar{v}(t, z) = \bar{v}_0(t) + (\bar{v}_L(t) - \bar{v}_0(t)) \frac{z}{L} \quad (11)$$

Macroscopic version of Eq. (2) for a pipe

We estimate the macroscopic variables by integrating Eqs. (2) and (3). First we calculate the average of Eq. (2) through a cross section of the pipe or joint by multiplying by $(2\pi r)/(\pi R(t)^2)$ and integrating in r :

$$\begin{aligned} & \int_0^{R(t)} \frac{2r}{R(t)^2} \frac{\partial v_z(t, r, z)}{\partial t} dr + \frac{1}{\pi R(t)^2} \int_0^{R(t)} 2\pi r \left(v_r \frac{\partial v_z}{\partial r} + v_z \frac{\partial v_z}{\partial z} \right) dr \\ &= - \int_0^{R(t)} \frac{2r}{R(t)^2} \frac{1}{\rho} \frac{\partial P(t, r, z)}{\partial z} dr + \frac{2\mu}{\rho R(t)} \left(\frac{\partial v_z}{\partial r} \right)_{(r=R(t))} \\ &+ \frac{\mu}{\pi \rho R(t)^2} \int_0^{R(t)} 2\pi r \frac{\partial v_z(t, z)}{\partial z^2} dr \end{aligned} \quad (12)$$

Using the continuity Eq. 4 we obtain

$$\begin{aligned} & \frac{\partial \bar{v}}{\partial t} + \frac{2\dot{R}(t)\bar{v}(t, z)}{R(t)} + \frac{4}{R(t)^2} \int_0^{R(t)} r v_z \frac{\partial v_z}{\partial z} dr \\ &= -\frac{1}{\rho} \frac{\partial \bar{P}}{\partial z} + \frac{2\mu}{\rho R(t)} \left(\frac{\partial v_z}{\partial r} \right)_{(r=R(t))}, \end{aligned} \quad (13)$$

where $\bar{P}(t, z)$ is the average pressure over the cross section at position z and time t .

Finally, we use the approximated velocity field and Eqs. (10) and (11), which yields the following equation:

$$\begin{aligned} & \frac{1}{2}(\dot{\bar{v}}_0(t) + \dot{\bar{v}}_L(t))L + \frac{5}{6}(\bar{v}_L^2(t) - \bar{v}_0^2(t)) \\ &= \frac{1}{\rho}(\bar{P}_0(t) - \bar{P}_L(t)) - \frac{4\mu L}{\rho R^2(t)}(\bar{v}_0(t) - \bar{v}_L(t)) \end{aligned} \quad (14)$$

Macroscopic version of Eq. (3) for a pipe

Next, we integrate Eq. (3) to obtain another differential equation for $(\dot{\bar{v}}_0(t), \dot{\bar{v}}_L(t))$. Equation (3) is multiplied by $\frac{r^2}{R^2}$, using the fact that $r^2 \frac{\partial P}{\partial r} = \frac{\partial}{\partial r}(r^2 P) - 2rP$, and integrated in r from 0 to $R(t)$; we get

$$\begin{aligned} & \frac{1}{R(t)^2} \int_0^{R(t)} \left(\frac{\partial v_r}{\partial t} + v_z \frac{\partial v_r}{\partial z} + v_r \frac{\partial v_r}{\partial r} \right) r^2 dr \\ &= -\frac{1}{\rho}(P_{\text{ext}}(t, z) - \bar{P}(t, z)) + \frac{\mu}{\rho R(t)^2} \\ & \quad \times \int_0^{R(t)} \left(\frac{1}{r} \frac{\partial}{\partial r} \left(r \frac{\partial v_r}{\partial r} \right) - \frac{v_r}{r^2} + \frac{\partial^2 v_r}{\partial z^2} \right) r^2 dr, \end{aligned} \quad (15)$$

where $P_{\text{ext}}(t, z) = P(t, R(t), z)$. Next we use the approximated velocity field (9) and integrate in z from 0 to L to obtain

$$\begin{aligned} & \frac{3R(t)^2(\bar{v}_L(t) - \bar{v}_0(t))^2}{32L} + \frac{R(t)^2(\dot{\bar{v}}_0(t) - \dot{\bar{v}}_L(t))}{6} \\ &= -\frac{L}{\rho} \bar{P}_{\text{ext}}(t) + \frac{1}{\rho} \int_0^L \bar{P}(t, z) dz + \frac{\mu}{\rho}(\bar{v}_L(t) - \bar{v}_0(t)) \end{aligned} \quad (16)$$

If the pressure gradient is not very high, we can make the approximation:

$$\int_0^L \bar{P}(t, z) dz \approx \frac{L}{2}(\bar{P}_0(t) + \bar{P}_L(t)) \quad (17)$$

Eqs. (14), (16), and (17) lead us to the ordinary differential equations that govern the dynamics of the pipe. These ODEs are

$$\dot{\bar{v}}_0(t) = \frac{3L(\bar{P}_L(t) + \bar{P}_0(t) - 2\bar{P}_{\text{ext}}(t))}{2\rho R(t)^2} - \frac{\mu(\bar{v}_L(t) + 7\bar{v}_0(t))}{\rho R(t)^2} \quad (18)$$

$$+ \frac{53\bar{v}_0(t)^2 - 107\bar{v}_L(t)^2 + 54\bar{v}_L(t)\bar{v}_0(t)}{96L} + \frac{\bar{P}_0(t) - \bar{P}_L(t)}{\rho L}, \quad (19)$$

$$\dot{\bar{v}}_L(t) = \frac{3L(\bar{P}_L(t) + \bar{P}_0(t) - 2\bar{P}_{\text{ext}}(t))}{2\rho R(t)^2} - \frac{\mu(7\bar{v}_L(t) + \bar{v}_0(t))}{\rho R(t)^2} \quad (20)$$

$$+ \frac{-53\bar{v}_L(t)^2 - 107\bar{v}_0(t)^2 - 54\bar{v}_L(t)\bar{v}_0(t)}{96L} + \frac{\bar{P}_0(t) - \bar{P}_L(t)}{\rho L} \quad (21)$$

Appendix 2

In this appendix we will describe the currents utilized in the neuron model. We will use the function $\Gamma(x, y, z)$ to introduce the activations and inactivations in all used currents,

$$\Gamma(x, y, z) = \frac{1}{1 + e^{\frac{z-y}{x}}}$$

The activation m and inactivation n of the ionic currents are governed by

$$\tau_m(V) \frac{dm}{dt} = m_\infty - m,$$

and

$$\tau_h(V) \frac{dh}{dt} = h_\infty - h$$

The axon currents are

- $I_{\text{Na}} = g_{\text{Na}} m^3 h(t)(V_f - 50)$, where m is a very fast activating variable. We set $m = m_\infty = \Gamma(-V_f, 4.5, 5.29)$, $h_\infty = \Gamma(V_f, -28.9, 5.18)$, $\tau_h = 0.67(1.5 + \Gamma(V_f, -14.9, 3.6)) \Gamma(-V_f, -42.9, 10.0)$, and $g_{\text{Na}} = 80 \mu\text{S}$.
- $I_{\text{Kd}} = g_{\text{Kd}} m^4 (V_f + 80)$, where $m_\infty = \Gamma(-V_f, -7.7, 11.8)$, $\tau_m = 7.2 - 6.4 \Gamma(-V_f, 8.3, 19.2)$, and $g_{\text{Kd}} = 30 \mu\text{S}$.
- $I_{\text{Lr}} = g_{\text{Lr}}(V_f + 65.0)$, with $g_{\text{Lr}} = 0.02 \mu\text{S}$.
- $I_{V_f, V_s} = g_{f_s}(V_s - V_f)$, with $g_{f_s} = 0.11 \mu\text{S}$.

The soma-neuropil currents are

- $I_{\text{Ca}} = g_{\text{Ca}} m^3 (V_s / (1 - \exp(2V_s/24.42)))$. Since the calcium concentration outside and inside are very different we used the Goldman-Hodgkin-Kotz description (see Hille 1992), $m_\infty = \Gamma(V_s, 21, 10)$, $\tau_m = 37.14 - 25.86\Gamma(-V_s, 10.1, 26.4)$ with $g_{\text{Ca}} = 1 \mu\text{S}$.
- $I_{\text{K(Ca)}} = g_{\text{K(Ca)}}(V_s + 80)([\text{Ca}]^4 / ([\text{Ca}]^4 + K_{\text{Ca}}^4))$ ($1/(1 + \exp((-V_s - 36)/15))$)($V_s + 80$), where $g_{\text{K(Ca)}} = 0.25 \mu\text{S}$ and $K_{\text{Ca}} = 0.4 \mu\text{M}$. We assumed again that m is rapidly activated.
- $I_h = g_h m(V_s + 15)$, where $m_\infty = \Gamma(V_s, -50.3, 10.5)$, $\tau_m = 7.2 - 6.4 \Gamma(-V_s, 8.3, 19.2)$, and $g_h = 2.1 \mu\text{S}$.
- $I_{\text{Ls}} = g_{\text{Ls}}(V_s + 65)$, with $g_{\text{Ls}} = 0.0024 \mu\text{S}$.

The dynamics of the bound receptors, r , is given by the equation

$$\frac{dr}{dt} = \alpha \cdot [T](1 - r) - \beta r,$$

where $[T]$ is the concentration of the transmitter, which occurs as a pulse; that is, $[T] = 1 \mu\text{M}$ for $t_0 < t < t_1$ and $[T] = 0 \mu\text{M}$ elsewhere. The spike is delivered by the axon at time t_0 , and $t_1 - t_0 = 2$ ms. The rise and decay constants are $\alpha = 10^4 \text{ms}^{-1} \mu\text{M}^{-1}$ and $\beta = 2 \cdot 10^{-4} \text{ms}^{-1}$.

To model the electrical activity of the muscles we used a passive circuit described by

$$C_m^{\text{muscle}} \frac{dV_m}{dt} = -g_L(V_m + 65 \text{mV}) + I^{\text{axon}}$$

where $g_L = 0.024 \mu\text{S}$, and I^{axon} is the excitatory input from the motor neurons, which is governed by the synaptic equations with the reverse potential set to 0 mV, $t_1 - t_0 = 1.5$ ms, $\alpha = 0.94 \text{ms}^{-1} \mu\text{M}^{-1}$ and $\beta = 0.18 \text{ms}^{-1}$.

References

- Abarbanel HDI, Huerta R, Rabinovich MI, Rulkov NF, Rowat PF, Selverston AI (1996) Synchronized action of synaptically coupled chaotic model neurons. *Neural Comput* 8:1567–1602
- Arshavsky YI, Beloozerova IN, Orlovsky GN, Panchin YV, Pavlova GA (1985) Control of locomotion in marine mollusc *Clio-limacina*. II. Rhythmic neurons of pedal ganglia. *Exp Brain Res* 58:263–272
- Arshavsky YI, Deliagina TG, Orlovsky GN (1997) Pattern generation. *Curr Opin Neurobiol* 7:781–789
- Bohm H (1996) Activity of the stomatogastric system in free-moving crayfish, *orcoctes-limosus* raf. *Zool Anal Complex Syst* 99:247–257
- Brodfehner PD, Debski EA, O’Gara BA, Friesen WO (1995) Neuronal control of leech swimming. *J Neurobiol* 27:403–418

- Clemens S, Massabau JC, Legeay A, Meyrand, P, Simmers J (1998) In vivo modulation of interacting central pattern generators in lobster stomatogastric ganglion: influence of feeding and partial pressure of oxygen. *J Neurosci* 18:2788–2799
- Cohen AH, Ermentrout GB, Kiemel T, Kopell N, Sigvardt KA, Williams TL (1992) Modeling of intersegmental coordination in the lamprey central pattern generator for locomotion. *Trends Neurosci* 15:434–438
- Collins JJ, Stewart I (1994) A group-theoretic approach to rings of coupled biological oscillators. *Biol Cybern* 71:95–103
- Cruse H, Brunn D, Bartling Ch, Dean J, Dreifert M, Kindermann T, Schmitz J (1995a) Walking: a complex behavior controlled by simple networks. *Adapt Behav* 3:385–419
- Cruse H, Bartling C, Cymbalyuk GDJ, Dreifert M (1995b) A modular artificial neuralnet for controlling a 6-legged walking system. *Biol Cybern* 72:421–430
- Delcomyn F (1980) Neural basis of rhythmic behavior in animals. *Science* 210:492–498
- Destexhe A, Mainen ZF, Sejnowski TJ (1994) An efficient method for computing synaptic conductances based on a kinetic model of receptor binding. *Neural Comput* 6:14–18
- Ekeberg O (1993) A combined neuronal and mechanical model of fish swimming. *Biol Cybern* 69:363–374
- Ekeberg O, Lansner A, Grillner S (1995) The neural control of fish swimming studied through numerical simulations. *Adap Behav* 3:363–385
- Elson RC, Maher M, Abarbanel HDI, Rabinovich MI, Selverston A (in press) Synchronization and regularization phenomena in coupled irregularly bursting neurons. I. Experimental studies. In: From physics to biology (Kluwer, Dordrecht) (eds) Enrique tirapequi and Servet Hontinen
- Falcke M, Huerta R, Rabinovich MI, Abarbanel HDI, Elson RC, Selverton AI (1998) Modeling observed chaotic oscillations in bursting neurons: the role of calcium dynamics and IP_3 (preprint)
- Giles RV, Evett JB, Liu C (1994) Schaum's outline of fluid mechanics and hydraulics. McGraw-Hill, New York
- Golowasch J, Marder E (1992) Ionic currents of the lateral pyloric neuron of the stomatogastric ganglion of the crab. *J Neurophysiol* 67(2):318–331
- Gottlieb GL, Latash ML, Corcos DM, Liubinskas TJ, Agarwal GC (1992) Organizing principles for single joint movements: V. Agonist-antagonist interactions. *J Neurophysiol* 67:1417–1427
- Grillner S, Deliagina T, Ekeberg O, El Manira A, Hill RH, Lansner A, Orlovsky GN, Wallen P (1995) Neural networks that coordinate locomotion and body orientation in lamprey. *Trends in Neurosci* 18:270–279
- Grillner S (1997) Ion channels and locomotion. *Science* 278:1087–1088
- Harris-Warrick RM, Coniglio LM, Levini RM, Gueron S, Guckenheimer J (1995) Dopamine modulation of two subthreshold currents produces phase shifts in activity of an identified motoneuron. *J Neurophysiol* 74:1404–1420
- Hatsopoulos NG (1996) Coupling the neural and physical dynamics in rhythmic movements. *Neural Comput* 8:567–581
- Hille B (1992) Ionic channels of excitable membranes. Sinauer Associates, Sunderland, Massachusetts
- Huerta R (1996) A finite automata model of spiking-bursting neurons. *Int J Bifurcation Chaos* 6:705–714
- Kandel ER, Schwartz JH, Jessel TM (1991) Principles of neural science, Elsevier, New York
- Katz PS, Harris-Warrick RM (1990) Actions of identified neuromodulatory neurons in a simple motor system. *J Neurosci* 10:1495–1512
- Katz PS, Getting PA, Frost WN (1994) Dynamic neuromodulation of synaptic strength intrinsic to a central pattern generator circuit. *Nature* 367:729–731
- Krylow AM, Sandercock TG, Rymer WZ (1995) Muscle models. In: Arbib MA (ed) The handbook of brain theory and neural networks. The MIT Press, Cambridge, Mass, 609–613
- Landau LD, Lifshitz EM (1963) Course of theoretical physics. (vol 6: fluid mechanics) Pergamon Press, London
- Liaw JS, Weerasuriya A, Arbib MA (1994) Snapping: a paradigm for modeling coordination of motor synergies. *Neural Netw* 7:1137–1152
- Marder E, Calabrese RL (1996) Principles of rhythmic motor pattern generation. *Physiol Rev* 76:687–717
- Morris LG, Hooper SL (1998) Muscle response to changing neuronal input in the lobster (panulirus-interruptus) stomatogastric system. Slow muscle properties can transform rhythmic input into tonic output. *J Neurosci* 18(9):3433–3442
- Müller-Wilm U, Dean J, Cruse H, Weidemann HJ, Eltze J, Pfeiffer F (1992) Kinematic model of a stick insect as an example of a 6-legged walking system. *Adaptive Behav* 1:33–46
- Rabinovich MI, Abarbanel HDI, Huerta R, Elson R, Selverston A (1997) Self-regularization of chaos in neural systems: experimental and theoretical results. *IEEE Trans Circuits Syst* 44:997–1005
- Roberts PD (1997) Classification of rhythmic patterns in the stomatogastric ganglion. *Neuroscience* 81:281–296
- Ryckebusch S, Laurent G (1993) Locomotor rhythms evoked in locust thoracic ganglia by the muscarinic agonist pilocarpine. *J Neurophysiol* 69:1583–1595
- Ryckebusch S, Laurent G (1994) Interactions between segmental leg central pattern generators during fictive rhythms in the locust. *J Neurophysiol* 72:2771–2785
- Ryckebusch S, Wehr M, Laurent G (1994) Distinct rhythmic locomotor patterns can be generated by a simple adaptive neural circuit: biology, simulation and VLSI implementation. *J Comput Neurosci* 1:339–358
- Schöner G (1995) Recent developments and problems in human movement science and their conceptual implications. *Ecol Psychol* 7:291–314
- Schöner G, Kelso JAS (1988) Dynamic pattern generation in behavioral and neural systems. *Science* 239:1513–1520
- Selverston AI, Moulins M (1985) Oscillatory neural networks. *Annu Rev Physiol* 47:29–48
- Selverston AI, Moulins M (1987) The crustacean stomatogastric system. Springer, Berlin Heidelberg New York
- Shaw BK, Kristan WB (1997) The neuronal basis of the behavioral choice between swimming and shortening in the leech: control is not selectively exercised at higher circuit levels. *J Neurosci* 17:786–795
- Sherwood DE, Schmidt RA, Walter CB (1988) Rapid movement with reversals in direction: I. The control of movement amplitude and inertial load. *Exp Brain Res* 69:355–367
- Sigvardt KA, Mulloney B (1982) Sensory alteration of motor patterns in the stomatogastric nervous system of the spiny lobster *Panulirus interruptus*. *J Exp Biol* 97:153–168
- Smith JC (1997) Integration of cellular and network mechanisms in mammalian oscillatory motor circuits: insights from the respiratory oscillator. In: Stein PSG, Grillner S, Selverston A, Stuart DG (eds) Neurons networks and motor behavior. MIT Press, Cambridge, Mass, pp 97–104
- Turrigiano G, LeMasson G, Marder E (1995) Selective regulation of current densities underlies spontaneous changes in the activity of cultured neurons. *J Neurosci* 15:3640–3652
- Wadden T, Hellgren J, Lansner A, Grillner S (1997) Intersegmental coordination in the lamprey – simulations using a network model without segmental boundaries. *Biol Cybern* 76:1–9
- Wolf H, Laurent G (1994) Rhythmic modulation of the mechanosensory receptive fields of locust spiking local interneurons by walking pattern generating networks. *J Neurophysiol* 71:110–118
- Zielinska T (1996) Coupled oscillators utilised as gait rhythm generators of a two-legged walking machine. *Biol Cybern* 74:263–273